crystals

MDPI

Article

Structural Evolution in a Series of Isomorphous Rare Earth Compounds as Response of Lanthanide Contraction

Hans Reuter *, Marcel Böltken, Maik Horstmann and Markus Haase

Chemistry, Department of Biology/Chemistry, Osnabrück University, Barbarastr. 7, 49069 Osnabrück, Germany
* Correspondence: hreuter@uos.de

Abstract: The structural parameters of the rare-earth diacetate halide trihydrates, $RE(OAc)_2Hal{\cdot}3H_2O$ with RE = Ce − (Pm) − Lu and Hal = Cl, Br, have been determined by low temperature, high-resolution SCXRD in order to examine the effect of lanthanide contraction on the coordination geometry in this series of isomorphous compounds consisting of cationic, acetate-bridged, non-linear, one-dimensional coordination polymers of composition $[RE(H_2O)_3(OAc)_2]^+$ and laterally hydrogen bonded halide ions, Hal^-. Although the shrinkage of the unit cell volume follows lanthanide contraction very well over the complete range of investigated RE elements, many other parameters (i.e., lattice constants, angles and distances in the RE··· RE alignment, RE-O bond lengths, etc.) exhibit a more complex response on lanthanide contraction often expressed by sigmoid curves that can be ascribed to a continuous transition from CN9 (RE = Ce) to CN8 (RE = Lu) as one acetate group loses the chelate function, an effect accompanied by significant structural changes of the carboxylate group. Therefore, data are best analyzed by use of two subsets represented by the two different structure types of Ce and Lu, the structural features of which change with decreasing/increasing the size of RE^{3+}, up to the borderline between both subsets.

Keywords: lanthanide contraction; coordination modes; coordination number; rare-earth compounds; acetates; coordination polymer; regression analysis; hydrogen bonds; rod stacking

Citation: Reuter, H.; Böltken, M.; Horstmann, M.; Haase, M. Structural Evolution in a Series of Isomorphous Rare Earth Compounds as Response of Lanthanide Contraction. *Crystals* **2023**, *13*, 1043. https://doi.org/10.3390/cryst13071043

Academic Editor: László Kovács

Received: 9 June 2023
Revised: 22 June 2023
Accepted: 26 June 2023
Published: 30 June 2023

1. Introduction

In the chemistry of the rare-earth elements, RE, usually comprising the elements of the scandium group (Sc, Y, La) and lanthanides (Ln = Ce to Lu), oxidation state +III plays an important role. Within this group the lanthanide contraction, the shrinkage of atomic and ion radii of Ln with increasing atomic number *Z* as a result of the lower shielding of the valence orbitals through the diffuse 4f orbitals is a well-known phenomenon not only responsible for the chemical similarity of these elements but also for the nearly identical atomic radii of the second- and third-row d-block elements. In the case of the pure lanthanide metals with valence electron configuration $(6s)^2(5d)^1(4f)^n(6p)^0$, contraction of the metal atom radii [1] exhibits discontinuities for Ln = Eu, Yb as a result of their half-filled and full-filled, respectively, 4f orbitals, but for Ln^{3+} ions the ionic radii [2] decrease continuously without interruption from 1.196 Å for Ce to 1.032 Å for Lu (Figure 1, Table S1). With RE^{3+} ionic radii of 1.075, and 1.216 Å the two rare-earth elements Y and La blend in quite well with the other RE elements while the much smaller element Sc [$r(Sc^{3+})$ = 0.87 Å, CN8] takes an exceptional position.

On the other side, the coordination number, CN, is strongly correlated to the size of a specific metal atom. The highest possible CN this metal atom can achieve in a given oxidation state strongly correlates with its size: the bigger the atom the higher its maximal accessible CN. Consequently, the larger RE elements should expose larger coordination numbers than the smaller ones in a series of isomorphous compounds.

This relationship between lanthanide contraction and coordination number is the reason why the existence range of RE^{3+} compounds of identical composition is sometimes

limited to some few, direct neighboring RE elements and why certain rare-earth compounds with identical composition occur in different structure types.

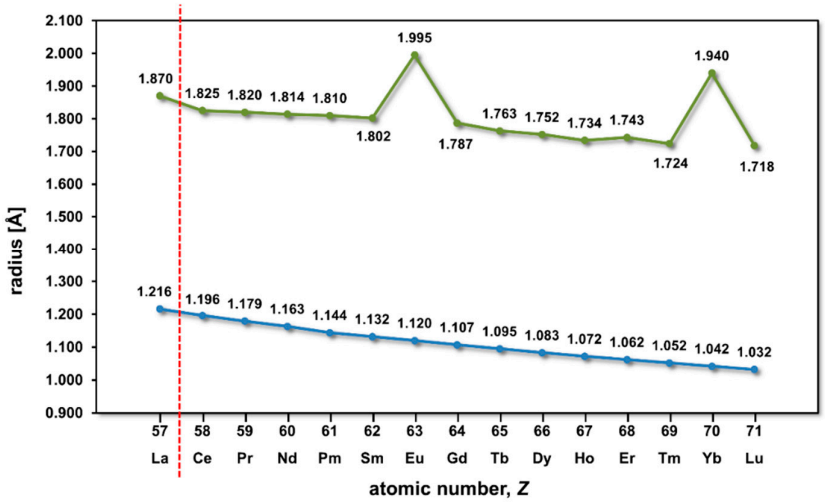

Figure 1. Evolution of atomic radii [1] and effective RE^{3+} ionic radii [2] throughout the series of rare earth elements of the 6th period PSE as a function of the atomic number, *Z*; dotted, vertical line (red) indicating the boundary between lanthanides and the element La of the scandium group.

In case of mononuclear RE^{3+} coordination compounds, this relationship is less pronounced especially with small, unidentate ligands such as H_2O, as the classical examples of RE(III) ethylsulfates, $[RE(H_2O)_9][EtO\text{-}SO_3]_3$, RE = La, Ln without Pm, CN9 [3]), and trifluoromethansulfonates, $[RE(H_2O)_9][CF_3\text{-}SO_3]_3$, RE = La, Ln without Pm, Ho, Er, Tm, CN9 [4]) prove. In both series of compounds crystal structure determinations confirm at both ends CN9 and tricapped trigonal-prismatic coordination of the RE^{3+} ion.

The relationship becomes more important in di- and polynuclear RE^{3+} coordination compounds, especially with bidentate, bridging ligands such as the acetate group, OAc: the existence range of *rare earth triacetate tetrahydrates*, $RE(OAc)_3{\cdot}4H_2O$ (dimeric, CN9, monocapped square antiprismatic), i.e., is well-documented by SCXRD only for RE = Sm − Lu [5–7], whereas two different structure types (Ho-structure type, CN8, bicapped trigonal-prismatic, RE = Sm − Er, Y [8]; Lu-structure type, CN7, monocapped trigonal-prismatic RE = Tm − Lu, [8]) dominate the structure chemistry of the pure *rare earth triacetates*, $RE(OAc)_3$.

In literature, a remarkable exception from this trend is documented for the *rare-earth diacetate chloride trihydrates*, $RE(OAc)_2Cl{\cdot}3H_2O$. Their crystallographic data [RE = Ce − (Pm)-Lu, Y] obtained from X-ray powder diffraction at room temperature [9] refer to a series of isomorphous compounds, whereas some few single crystal structure determinations (RE = Eu [10], Gd [11], and Tb = [12]) demonstrate that their structures are built up of one-dimensional coordination polymers with bridging acetate ligands and CN9 of the RE atoms. With 13/14 data points of RE (as usual, Pm was not investigated because of its radioactivity), this set of compounds provides the best preconditions to study the influence of lanthanide contraction on the structural evolution within a given class of polymeric RE^{3+} coordination compounds where one expects a reduction of the coordination number from the lightest/largest (Ce) to heaviest/smallest (Lu) rare-earth metal [9].

By chance, we become aware of this class of compounds when searching for improved crystallization conditions of anhydrous *rare-earth triacetates* as precursors in the synthesis of $NaREF_4$ and $LiYF_4$ core and core/shell nanocrystals [13]. When recrystallizing $Eu(OAc)_3 \cdot xH_2O$, originally prepared via the reaction sequence $EuCl_3{\cdot}6H_2O - Eu_2O_3 - Eu(OAc)_3$, we found a few single crystals of $Eu(OAc)_2Cl{\cdot}3H_2O$ as side product obviously resulting from the uncomplete chloride-to-oxide transformation.

As the above-mentioned single crystal X-ray structure determinations have been performed using different measurement strategies at different temperatures [295 K, Eu; 150 K, Gd; 123 K, Tb] and as the atomic radii of their rare-earth elements are just in the middle of those from Ce and Lu, we decided to perform a systematic study on the crystal structures of these class of compounds applying uniform measurement conditions in order to obtain comparable and valid data. In addition, we extended the existence range of the class of *rare-earth diacetate halide trihydrates*, $RE(OAc)_2Hal{\cdot}3H_2O$, to those with Hal = Br.

2. Materials and Methods

2.1. Preparation

All compounds can easily be prepared by solving anhydrous, $RE(OAc)_3$, hydrated, $RE(OAc)_3 \cdot nH_2O$, or acetic acid solvated, $RE(OAc)_3 \cdot n$AcOH, rare-earth triacetates in acetic acid, $AcOH_{(aq)}$, and addition of diluted hydrochloric, $HCl_{(aq)}$, or hydrobromic, $HBr_{(aq)}$, acid in a molar ratio of 1:1. A typical reaction equation based on the use of a *tetrahydrate* is sketched out in Scheme 1. Additional procedures for the preparation of the chlorides are described in the literature [9].

$$RE(OAc)_3 \cdot 4H_2O + HHal_{(aq)} \xrightarrow{AcOH(aq)} RE(OAc)_2Hal \cdot 3H_2O + AcOH_{(aq)} + H_2O$$

Scheme 1. Reaction equation for the formation of rare-earth diacetate bromide trihydrates by use of tetrahydrates as starting material.

With adhesive solvent, crystals are very sensitive towards moisture free of remaining solvent; they are stable at ambient conditions over periods of hours and days. For X-ray diffraction experiments, crystals have been selected without drying; for elemental analyses and spectroscopic measurements, they have been dried between two filtering papers.

All compounds have been characterized with respect to their C and H content. Mid-infrared and Raman spectra have been recorded for RE = Tb, Dy, Ho, Er, Tm, Yb, Lu, and both halides. These spectra are very similar with only slight differences in wavenumbers and intensities.

All compounds constitute transparent, colorless crystals without those of Yb (pink), and Pr (greenish). Crystal morphology is characterized by a prismatic habit (Figure 2) resulting from the combination of the pinacoids {100}, {010}, and {001}, often elongated along the a-axis, the propagation direction of the coordination polymer (see below).

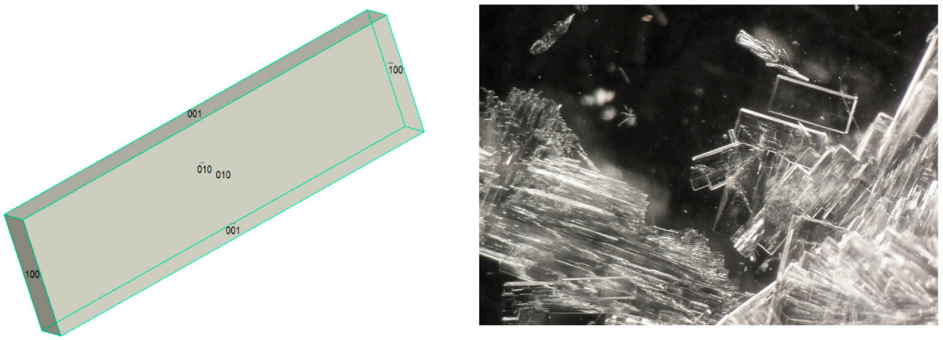

Figure 2. Typical prismatic shape (**left**) of crystals of $RE(OAc)_2Hal{\cdot}3H_2O$ compounds (here: greenish crystals of RE = Pr, Hal = Cl), and microscopic image (**right**) showing an assemblage (here: RE = Lu, Hal = Cl) of crystals in the mother liquor.

Typical procedure: 205.0 mg (0.5 mmol) $Tb(OAc)_3 \cdot 4H_2O$ are dissolved in a 50 mL roll-rim glass by stirring at ambient temperature in about 20 mL concentrated acetic acid, $AcOH_{(aq)}$, before 0.5 mL of 1M hydrobromic acid (0.5 mmol) are added via a syringe. Thereafter, the excess of water and acetic acid is allowed to evaporate at atmosphere up to the crystallization of $Tb(OAc)_2Br{\cdot}3H_2O$.

Analysis (found/calc): C = 12.97/13.11%, H = 3.18/3.30%.

MIR spectrum: (Figure S1)
Raman spectrum: (Figure S2)

2.2. Spectroscopic Measurement and Elemental Analyses

Mid-infrared spectra were collected on a VERTEX 70 Fourier transform IR spectrometer using the attenuated total reflectance (ATR) technique, Raman spectra with the Fourier transform Raman module RAM II (both: Bruker AXS GmbH, Karlsruhe, Germany). Carbon and hydrogen microanalyses were performed on a vario MICRO cube from Elementar Analysensysteme GmbH, Hanau, Germany.

2.3. Single Crystal X-ray Structure Determinations

Details of sample handling, single crystal X-ray equipment, data collection and processing, structure solution, and refinement have been described previously [13].

All H atoms including those of the water molecules were clearly identified in difference-Fourier syntheses. Hydrogen atoms of the methyl groups were refined with idealized positions and allowed to ride on their parent carbon atoms with d(C-H) = 0.98 Å and common isotropic temperature factors for all three hydrogen atoms of each methyl group. Whenever these values became extraordinarily large, the final difference in Fourier syntheses indicated hydrogen positions of a second methyl orientation. In these cases, both orientations have been included in the structure model with different site occupations but common (now smaller) isotropic temperature factors. Hydrogen atoms of the water molecules were refined with a common O-H distance of 0.96 Å and an angle of 104.95° before they were fixed and allowed to ride on the corresponding oxygen atom with common isotropic temperature factors.

Details on the crystallographic data, data collection parameters, and structure refinement results are summarized in Table 1 (Hal = Cl) and Table 2 (Hal = Br). The listed CCDC numbers contain the supplementary crystallographic data for this paper. These data can be obtained free of charge from the Cambridge Crystallographic Data Centre via https://www.ccdc.cam.ac.uk/structures (accessed on 25 June 2023). Additional tables of bond lengths and angles prepared by SHELXL [14], as well as the results of the structure validation program Checkcif [15] are documented for each compound in the supplementary data.

Molecular graphics were prepared using DIAMOND [16], Mercury [17], and POV-Ray [18], respectively. With the exception of the hydrogen atoms that were drawn as spheres of arbitrary radii, all other atoms are shown in ball-and-stick models as thermal displacement ellipsoids of the 50% level.

Table 1. Crystallographic data, summary of data collection parameters and results of structure refinement for $RE(OAc)_2Cl{\cdot}3H_2O$.

	Ce	**Pr**	**Nd**	**Pm**	**Sm**	**Eu**	**Gd**	**Tb**	**Dy**	**Ho**	**Er**	**Tm**	**Yb**	**Lu**
Empirical formula	$C_4H_{23}CeClO_7$	$C_4H_{12}ClO_7Pr$	$C_4H_{12}ClNdO_7$		$C_4H_{12}ClO_7Sm$	$C_4H_{12}ClEuO_7$	$C_4H_{12}ClGdO_7$	$C_4H_{12}ClO_7Tb$	$C_4H_{12}ClDyO_7$	$C_4H_{12}ClHoO_7$	$C_4H_{12}ClErO_7$	$C_4H_{12}ClO_7Tm$	$C_4H_{12}ClO_7Yb$	$C_4H_{12}ClLuO_7$
Formula weight [g/mol]	347.71	348.50	351.83		357.94	359.55	364.84	366.51	370.09	372.52	374.85	376.52	380.63	382.56
Temperature [K]		100(2)						100(2)						
Crystal system		monoclinic						Monoclinic						
Space group		$P\,2_1/n$						$P\,2_1/n$						
a [Å]	7.9625(3)	7.9333(3)	7.9059(3)		7.8503(3)	7.8412(2)	7.8219(4)	7.8003(2)	7.8106(4)	7.7993(3)	7.7927(3)	7.7747(2)	7.7710(3)	7.7668(3)
b [Å]	7.9276(3)	7.9139(3)	7.9008(3)		7.8844(3)	7.8769(2)	7.8592(4)	7.8539(2)	7.8433(4)	7.8345(3)	7.8301(5)	7.8392(2)	7.8224(3)	7.8297(3)
b [Å]	17.6973(6)	17.6327(6)	17.5852(7)		17.5192(6)	17.4901(5)	17.4434(8)	17.3942(5)	17.3400(8)	17.2564(7)	17.1904(7)	17.1517(5)	17.1055(8)	17.0618(7)
β	99.122(2)°	98.947	98.856(2)		98.483(2)	98.354(1)°	98.265(2)	98.075(2)°	97.978(2)°	97.881(2)°	97.695(2)	97.552(1)	97.422(2)	97.336(2)
Volume [$Å^3$]	1102.99(7)	1093.57(7)	1085.33(7)		1072.49(7)	1068.80(5)	1061.18(9)	1055.05(5)	1051.98(9)	1044.47(7)	1039.47(7)	1036.28(5)	1031.09(7)	1029.06(7)
Z,Z′,d_{calc} [g/mol]	4, 1, 2.094	4, 1, 2.117	4, 1, 2.153		4, 1, 2.217	4, 1, 2.234	4, 1, 2.284	4, 1, 2.307	4, 1, 2.337	4, 1, 2.369	4, 1, 2.395	4, 1, 2.413	4, 1, 2.452	4, 1, 2.469
μ [mm^{-1}]	4.373	4.703	5.034		5.728	6.122	6.509	6.960	7.361	7.835	8.335	8.823	9.333	9.857
F(000)	668	672	676		684	688	692	696	700	704	708	712	716	720
$2\Theta_{max}$		56°							56°					
Reflections collected	101277	125986	122829		130814	79828	122742	126109	49237	133421	93.617	108715	70583	100183
Reflections unique, R_{int}	2664, 0.0460	2645, 0.0398	2621, 0.0566		2595, 0.0344	2587, 0.0399	2569, 0.0358	2551, 0.0517	2547, 0.0328	2528, 0.0358	2514, 0.0305	2504, 0.0397	2491, 0.0721	2490, 0.0653
Data/restraints/ parameters	2664/0/125	2645/0/125	2621/0/125		2595/0/126	2587/0/125	2569/0/126	2551/0/125	2547/0/126	2528/0/126	2514/0/126	2504/0/125	2491/0/125	2490/0/125
Goodness of fito n F^2	1.224	1.101	1.062		1.133	1.094	1.090	1.054	1.184	1.176	1.409	1.132	1.061	1.034
R1/wR2 [I > 2σ(I)]	0.0177, 0.0355	0.0125, 0.0280	0.0122, 0.0270		0.0101, 0.0233	0.0131, 0.0327	0.0094, 0.0206	0.0108, 0.0245	0.0127, 0.0266	0.0103, 0.0234	0.0135, 0.0292	0.0108, 0.0240	0.0162, 0.0302	0.0119, 0.0264
R1/wR2 [all data]	0.0186, 0.0358	0.0134, 0.0283	0.0142, 0.0275		0.0105, 0.0235	0.0137, 0.0330	0.0100, 0.0208	0.0131, 0.0253	0.0131, 0.0267	0.0106, 0.0235	0.0135, 0.0292	0.0113, 0.0241	0.0217, 0.0318	0.0143, 0.0269
Extinction coefficient		N/A			0.00104(8)	N/A	0.00122(7)	N/A	0.0045(1)	0.00185(8)	0.00115(9)		N/A	
±Δe[$eÅ^{-3}$]	0.532/−0.811	0.457/−0.609	0.387/−0.358		0.381/−0.528	0.470/−0.703	0.348/−0.474	0.486/−0.392	0.489/−0.652	0.364/−0.436	0.524/−0.603	0.386/−0.579	0.522/−0.480	0.365/−0.421
CCDC number	2260824	2260831	2260827		2260830	2260822	2260828	2260829	2260820	2260832	2260823	2260825	2260821	2206826

Table 2. Crystallographic data, summary on data collection parameters and results of structure refinement for $RE(OAc)_2Br{\cdot}3H_2O$.

	Ce	Pr	Nd	Pm	Sm	Eu	Gd	Tb	Dy	Ho	Er	Tm	Yb	Lu
Empirical formula	$C_4H_{23}BrCeO_7$	$C_4H_{12}BrO_7Pr$	$C_4H_{12}BrNdO_7$		$C_4H_{12}BrO_7Sm$	$C_4H_{12}BrEuO_7$	$C_4H_{12}BrGdO_7$	$C_4H_{12}BrO_7Tb$	$C_4H_{12}BrDyO_7$	$C_4H_{12}BrHoO_7$	$C_4H_{12}BrErO_7$	$C_4H_{12}BrO_7Tm$	$C_4H_{12}BrO_7Yb$	$C_4H_{12}BrLuO_7$
Formula weight [g/mol]	392.17	392.96	396.29		402.40	404.01	409.30	410.97	414.55	416.98	419.31	420.98	425.09	427.02
Temperature [K]		100(2)						100(2)						
Crystal system		monoclinic						Monoclinic						
Space group		$P\,2_1/n$						$P\,2_1/n$						
a [Å]	7.9597(3)	7.9293(3)	7.9027(3)		7.8473(3)	7.8318(3)	7.8191(2)	7.7972(3)	7.8038(3)	7.8117(3)	7.8069(3)	7.7868(5)	7.7854(3)	7.7611(3)
b [Å]	8.0442(3)	8.0327(3)	8.0349(3)		8.0230(3)	8.0121(3)	8.0130(2)	8.0263(3)	8.0288(3)	8.0361(4)	8.0529(3)	8.0675(5)	8.0625(3)	8.0702(3)
b [Å]	18.0642(8)	18.0186(6)	17.9481(6)		17.8722(7)	17.8214(7)	17.7804(6)	17.7443(8)	17.6550(7)	17.5440(9)	17.4494(7)	17.3994(7)	17.3573(7)	17.2952(6)
β	96.732(2)°	96.533(2)°	96.414(2)°	°	95.987(2)°	95.972(2)°	95.929(2)°	95.862(2)°	96.034(2)°	96.096(3)°	96.154(2)°	96.154(2)°	96.142(29)°	96.098(2)°
Volume [$Å^3$]	1148.67(8)	1140.22(7)	1132.52(7)		1119.08(7)	1112.21(7)	1108.06(5)	1104.68(8)	1100.05(7)	1095.11(9)	1090.69(7)	1086.73(11)	1083.26(7)	1077.13(7)
Z,Z′,d_{calc} [g/mol]	4, 1, 2.268	4, 1, 2.289	4, 1, 2.324		4, 1, 2.388	4, 1, 2.413	4, 1, 2.453	4, 1, 2.471	4, 1, 2.503	4, 1, 2.529	4, 1, 2.544	4, 1, 2.573	4, 1, 2.606	4, 1, 2.633
μ [mm^{-1}]	7.446	7.781	8.117		8.822	9.236	9.595	10.023	10.429	10.878	11.362	11.845	12.326	12.879
F(000)	740	744	748		756	760	764	768	772	776	780	784	788	792
$2\Theta_{max}$		56°						56°						
Reflections collected	113305	92529	132337		1113760	118192	132199	124829	101683	102663	121.468	112602	120213	103545
Reflections unique, R_{int}	2770, 0.0572	2753, 0.0497	2735, 0.0553		2708, 0.0701	2696, 0.0516	2690, 0.0410	2683, 0.0459	2666, 0.0444	2655, 0.0734	2636, 0.0413	2626, 0.0488	2616, 0.0460	2596, 0.0753
Data/restraints/ parameters	2770/0/125	2753/0/125	2735/0/125		2708/0/125	2696/0/125	2690/0/125	2683/0/125	2666/0/126	2655/0/125	2636/0/126	2626/0/125	2616/0/125	2596/0/125
Goodness of fito n F^2	1.071	1.078	1.051		1.084	1.100	1.134	1.122	1.118	1.049	1.182	1.083	1.073	1.054
R1/wR2 [I>2σ(I)]	0.0142, 0.0310	0.0141, 0.0295	0.0129, 0.0300		0.0150, 0.0305	0.0131, 0.0300	0.0155, 0.0403	0.0133, 0.0301	0.0129, 0.0321	0.148, 0.0336	0.0114, 0.0253	0.0118, 0.0265	0.0121, 0.0261	0.0184, 0.0417
R1/wR2 [all data]	0.0173, 0.0321	0.0175, 0.0305	0.0154, 0.0307		0.0201, 0.0321	0.0157, 0.0309	0.0168, 0.0410	0.0151, 0.0306	0.0140, 0.0325	0.196, 0.0353	0.0123, 0.0255	0.0141, 0.0272	0.0141, 0.0266	0.0233, 0.0437
Extinction coefficient		N/A				N/A			0.00126(9)	N/A	0.00082(5)		N/A	
±Δe[$eÅ^{-3}$]	0.368/−0.374	0.441/−0.499	0.402/−0.415		0.442/−0.443	0.408/−0.408	0.695/−0.977	0.554/−0.407	0.779/−0.601	0.508/−0.579	0.364/−0.467	0.383/−0.226	0.4607/−0.581	1.131/−1.209
CCDC number	2261207	2261199	2261203		2261208	2261206	2261205	2261209	2261200	2261198	2261201	2261202	2261204	2261210

3. Results and Discussion

Our single crystal X-ray measurements in the series of isomorphous $RE(OAc)_2Hal{\cdot}3H_2O$ compounds confirm the previous results of a cationic, non-linear, one-dimensional coordination polymer of composition $\{RE(H_2O)_3(\mu_2\text{-}OAc)_2\}^+$ with two different RE···RE-distances propagating along the a-axis of a monoclinic unit cell of space group $P2_1/n$ linked together via hydrogen bonds to the halide anions, Hal^-. Moreover, they show that a similar series of isomorphous compounds exist for Hal = Br, structurally related to the former one.

Atoms of all compounds were labeled according to the common numbering scheme depicted in Figure 3.

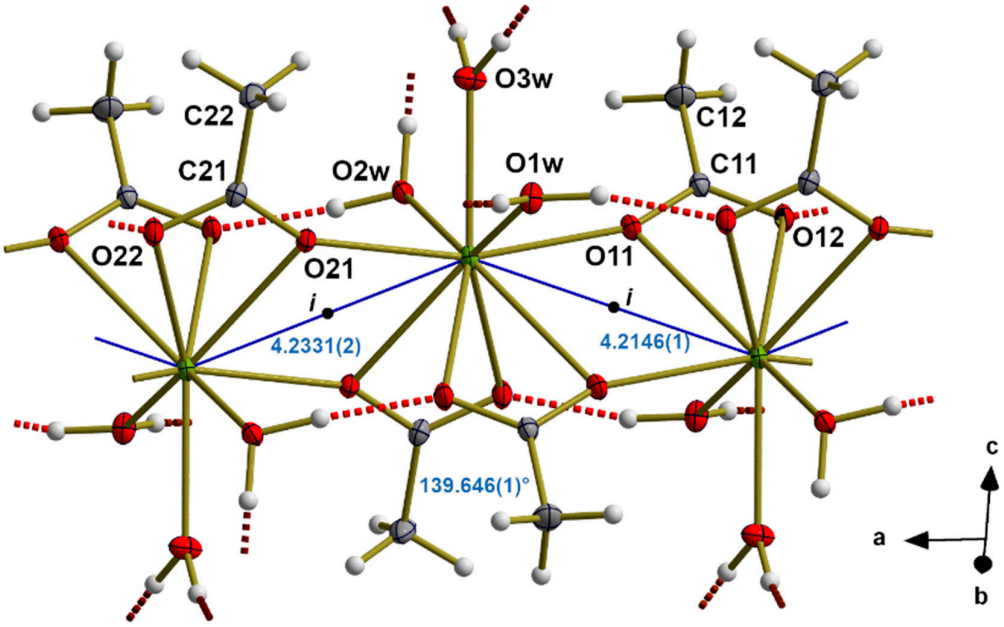

Figure 3. Ball-and-stick model showing the general building concept of the one-dimensional coordination polymers in the $RE(OAc)_2Hal{\cdot}3H_2O$ structure type (here: RE = Pr, Hal = Br) with atom labeling scheme of the asymmetric unit; hydrogen atoms not labeled and the position of the halide atom not shown for clarity; hydrogen bonds visualized as dashed sticks (-OH···H = red, -OH··· Br = brown) and covalent bonds to adjacent, symmetry-related atoms as shortened sticks; the non-linear, unsymmetrical arrangement of the RE atoms is visualized by blue lines with distances [Å] and angle; black dots labeled *i* show the positions of the crystallographic centers of symmetry.

3.1. Unit Cell Volumes and Lattice Parameters

In the two series of $RE(OAc)_2Hal{\cdot}3H_2O$ compounds, there are two different size effects with influence on the external (lattice parameters, unit cell volume) as well as internal (bond lengths, bond angle, hydrogen bonds, etc.) structural parameters: the size of the rare-earth elements, RE, and the size of the halide ion, Hal.

The progression of the unit cell volumes as a function of the atomic number of RE is shown in Figure 4. From the larger RE (CE) to the smallest one (Lu), the unit cell volumes decrease almost uniformly and to the same extent for both halides, Hal = Cl [$\Delta V_{Ce\text{-}Lu}$ = 73.93 Å^3] as well as Hal = Br [$\Delta V_{Ce\text{-}Lu}$ = 71.54 Å^3].

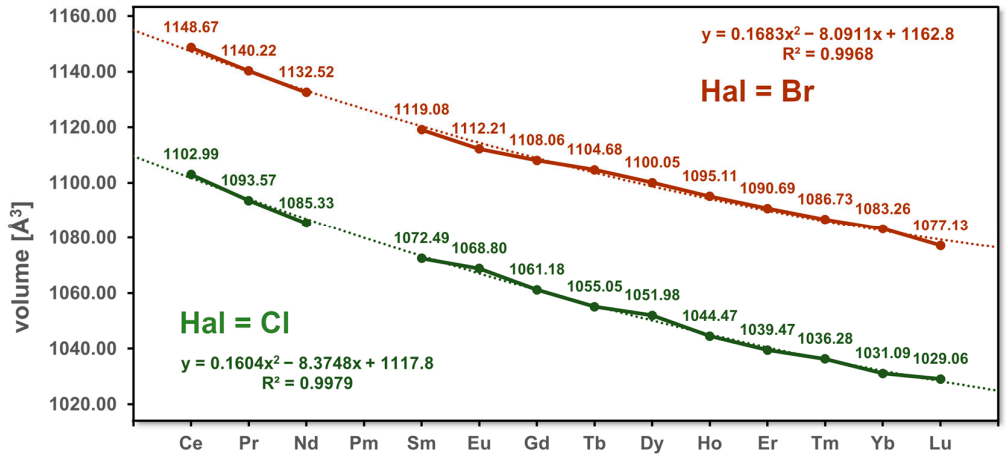

Figure 4. Unit cell volumes [Å^3] in the series of isomorphous RE(OAc)$_2$Hal·3H$_2$O compounds for Hal = Cl (dark green), and Hal = Br (brown); dotted lines represent the graphs of the quadratic regression analyses with parameters and reliability factors R given.

To visualize lanthanide contraction such graphs are usually fitted by use of linear [V(x) = Ax + B] or quadratic [V(x) = Ax^2 + Bx + C] regression analyses [19]. In the present case, linear regression analyses (Figure S3) result in quite well reliability factors $R_{Cl/Br}$ [0.9872/0.9831] but reveal systematic errors, too: volumes calculated using the fitting parameters are too large for the lighter and heavier RE elements and too small for elements in between (Figure S4). Even if these differences are very small and in the range of some permille they are significant and of the same kind and quantity in both series of halide compounds. In contrast, regression analysis by use of quadratic equations (Figure 4) works better [$R_{Cl/Br}$ = 0.9979/0.9968] and produces errors $\Delta V = V_{obs} - V_{calc}$ that only show a statistical distribution (Figure S5).

The difference $\overline{d}(V_{Br} - V_{Cl})$ between the unit cell volumes of compounds with the same RE but different halide ions amount to 48.3(25) Å^3. In the same extent as unit cell volumes decrease, densities increase [$R_{Cl/Br}$ = 0.9978/0.9988, quadratic equations].

Although the unit cell volumes reflect both the lanthanide contraction and the size of the different halide ions very well, changes in the lattice parameters must follow other rules, because the lanthanide contraction should predominate in the direction of the crystallographic a-axis (=the propagation axis of the coordination polymer) whereas the size of the halide ions interconnecting the coordination polymers via hydrogen bonds should cause stacking variations with a larger influence on the lattice parameters b, c, and ß.

With respect to the a-axis, the size of the halide ions should have a negligible effect as they are not involved in the formation of the coordination polymer. Changes in lengths of a-axes with increasing atomic number *Z* of RE are graphically plotted in Figure 5 for both halides. As expected from lanthanide contraction, the length of this axis decreases significantly [$\Delta(a_{Ce} - a_{Lu})_{Cl/Br}$ = 0.1957/0.1986 Å] from RE = $Ce_{Cl/Br}$ [7.9625(3)/7.9597(3) Å] to RE = $Lu_{Cl/Br}$ [7.7668(3)/7.7611(3) Å]. Applying quadratic regression analyses over the complete datasets results in quite well R factors $R_{Cl/BR}$ [0.9885/0.9592]. Differences between observed and calculated values are very small for the early RE elements (Ce to Gd) but become larger for the late ones (Tb to Lu).

On the first view, one might suggest that the greater deviations at the right end of the diagram are caused by experimental errors perhaps resulting from absorption effects as the linear absorption coefficients $\mu(MoK_\alpha)$ increase with increasing *Z* of the RE element. A more detailed analysis taking into account the evolution of all sets of internal and external structural parameters (see below), however, shows that the response of the atom arrangement in the structures of the RE(OAc)$_2$Hal·3H$_2$O compounds on lanthanide contraction is more complex than expected and is inadequately described by use of only one fitting equation over the complete range of the 6f-bloc metals. Thus, most of the parameters analyzed in this paper show significant chances when comparing their progress

in the area of the early RE elements, *e*RE = Ce − Gd, with that in the area of the late ones, *l*RE = Tb − Lu, very similar to the situation just described for the a-axis. As a consequence, we will handle the data of both groups of RE elements separately throughout the paper whenever meaningful.

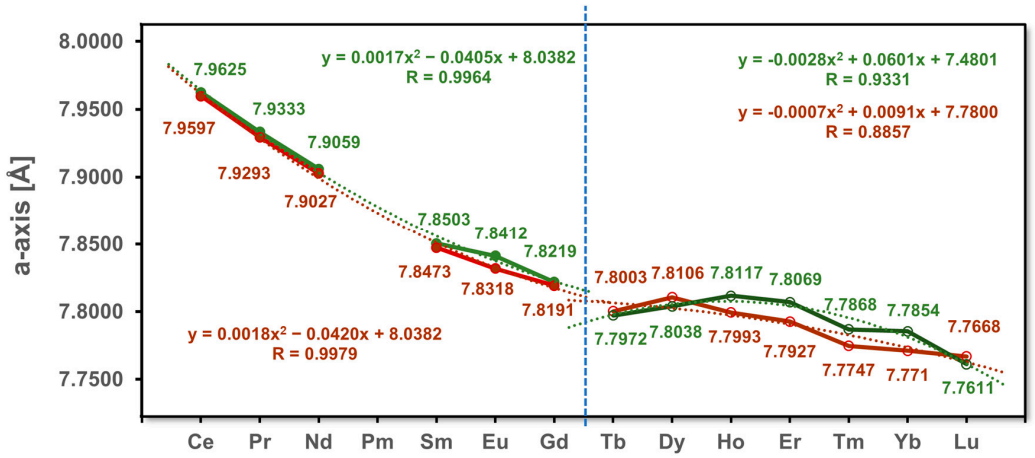

Figure 5. Variation of the a-axis [Å] in the $RE(OAc)_2Hal{\cdot}3H_2O$ compounds for Hal = Cl (dark red) and Hal = Br (brown) as a function of *Z*, by a horizontal, dotted line (blue).

In the case of the early RE elements, differences between a_{cl} and a_{Br} are very small (for Ce −Sm they are marginal), and both series can be fitted with high reliability [$R_{Cl/Br}$ = 0.9964/0.9979] by use of quadratic equations (Figure 5) for the convex curvatures. In the case of the late RE elements, the graphs, however, display concave curvatures. On the foregoing statements, this contrary behavior seems implausible but becomes more reasonable when taking into account that the alignment of the RE atoms (distances, angles) in the coordination polymer acts as a further adjusting screw to bring lanthanide contraction, coordination geometry, and hydrogen bonded halide ions into structural balance. Obviously, these interactions are very complex in the case of the late RE elements as even the quadratic regression analyses of the data are of limited precession [$R_{Cl/Br}$ = 0.9331/0.8857]

As mentioned above, all other lattice parameters should be much more infected by the size of the halide ion as they crosslink the individual rods of coordination polymers via hydrogen bonds in the bc-plane.

The lengths of the c-axes (Figure S6) decrease with decreasing size of RE, too, from 17.6973(6)/18.0642(8) Å for RE = $Ce_{Cl/Br}$ to 17.0618(7)/17.2952(6) Å for RE = $Lu_{Cl/Br}$. The decrease is independent of the halide ion, but for Hal = Br lengths of the c-axes are longer [from 0.3859 Å for Pr up to 0.2334 Å for Lu] than for Hal = Cl. In both subsets, data can be fit very reliably with quadratic equations [$R_{Cl/Br}$(*e*RE) = 0.9922/0.9961, $R_{Cl/Br}$(*l*RE) = 0.9960/0.9955].

Much more complex behavior is observed for the b-axes (Figure S7). For Hal = Cl the length of the b-axis decreases slightly [Δb(Cl) = −0.0979 Å] from Ce [7.9276(3) Å] to Lu [7.8297(3) Å]. The b-axes are longer for Hal = Br than for Hal = Cl but in contrast to the c-axis the differences between both increase from RE = Ce [0.1166 Å] to Lu [0.2405 Å]. This is due to the fact that the lengths of the b-axis increase with decreasing size of RE from 8.0442(3) Å for Ce to 8.0702(3) Å, RE = Lu for Hal = Br [Δb(Br) = +0.026 Å]. When fitting the data of both sectors using quadratic equations the reliability factors are moderate in the case of the early RE elements [$R_{Cl/Br}$(eRE) = 0.9856/0.9334] but poor [$R_{Cl/Br}$(LRE) = 0.7738/0.9220] in the case of the late RE elements reflecting a complicated interaction between the structure constituting building units.

The foregoing statement becomes obvious when analyzing the monoclinic angle ß (Figure S8). First, ß is always smaller for Hal = Br than for Hal = Cl. The difference between both decreases from RE = Ce [$\Delta ß_{Br/Cl}$ = 2.39°] to RE = Lu [$\Delta ß_{Br/Cl}$ = 1.24°] as the decrease of the absolute values [$\Delta ß = ß_{Ce} - ß_{Lu}$] between Ce and Lu is less expressed for Hal = Br

[Δß = 0.63°] than for Hal = Cl [Δß = 1.79°]. As before the dataset of the chlorides can be split into two separate datasets but there is no need as the R-value [0.9977] of the quadratic regression analysis over the complete series of RE elements is excellent. Splitting, however, is obviously necessary for the data of the bromides [R = 0.8347, complete dataset, quadratic equation]. For *e*RE, these data show a concave curvature, and those of *l*RE show a convex one resembling the course of the a-axis in this subset. The corresponding fits are acceptable [$R_{eRE/lRE}$ = 0.9805/0.9796, quadratic equation].

3.2. Alignment of RE in the Coordination Polymer

The first information about the response of the atom arrangement in the $RE(OAc)_2Hal{\cdot}3H_2O$ structure on the shrinkage of the ion radius with increasing Z results from the alignment of the RE atoms within the coordination polymer. Its repeat unit is characterized by two different interatomic RE···RE distances and one angle, ∠(RE···RE···RE), resulting from the non-linear arrangement of the RE atoms. The shorter of both interatomic distances, $d(RE{\cdots}RE)_{short}$, results from the bridging via the acetate ligand OAc_2 (atoms O21-C22, see below), the longer one, $d(RE{\cdots}RE)_{long}$, from the bridging via acetate group OAc_1 (atoms O11-C12, see below). The corresponding data as a function of increasing Z are summarized in Table S2 and visualized in Figure 6.

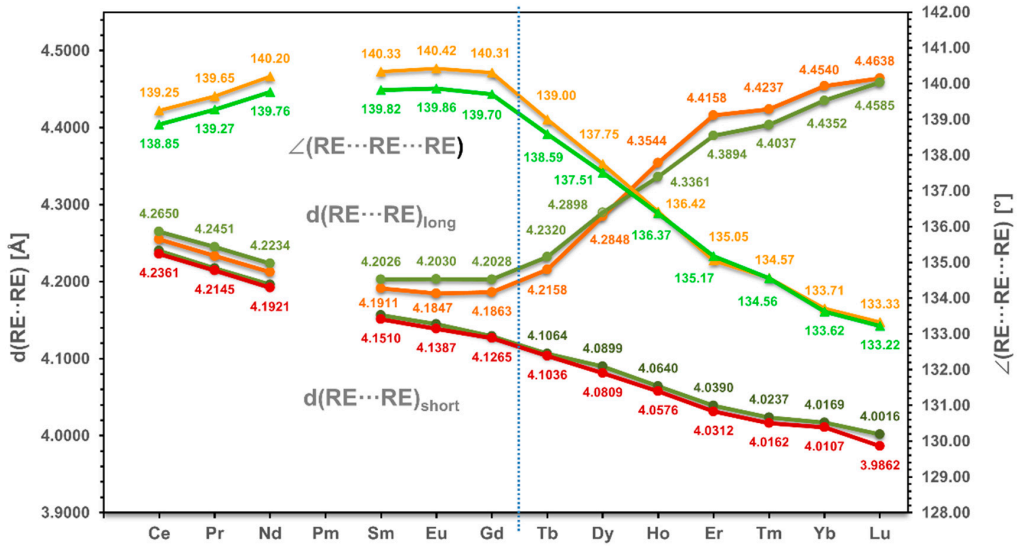

Figure 6. Distances [Å], and angles [°] between the RE atoms in the $RE(OAc)_2Hal{\cdot}3H_2O$ compounds with Hal = Cl (dark green, olive, green), and Hal = Br (dark red, brown, orange), for reasons of clarity all curves are drawn over the complete datasets without interruption at the borderline (dotted, blue) between the early and late RE elements.

At first glance, $d(RE{\cdots}RE)_{short}$ decreases continuously with decreasing size of RE from $Ce_{Cl/Br}$ = 4.2361/4.2549 Å to $Lu_{Cl/Br}$ = 3.9862/4.0016 Å [$\Delta_{Cl/Br}d(RE{\cdots}RE)_{short}$ = 0.2499/0.2533 Å]. This parameter is almost independent of the size of the counterion and can adequately be described by a linear equation [$R_{Cl/Br}$ = 0.9953/0.9956] over the complete dataset.

Comparable RE···RE distances are found in many dimeric and polymeric RE coordination compounds. For the reason of comparability, we will restrict the discussion to pure acetate compounds measured exactly on the same conditions as in the present paper. Values from the literature may differ as a result of different measurement and refinement strategies. The relations between d(RE···RE) of $RE(OAc)_2Hal{\cdot}3H_2O$ to those in other RE acetate compounds are graphically represented in Figure S9. In the dimeric molecules of the *triacetate tetrahydrates* the curve of the RE···RE distances shows an almost similar behavior over the complete range of its existence range [RE = Sm − Lu] but with an offset of about +0.05 Å. In the one-dimensional coordination polymer of the *rare earth triacetate*

diacetic acid solvates, RE(OAc)$_3$ ·2AcOH with RE = Nd − Gd [13], the length of both different RE ···RE distances are of the same magnitude as the RE···RE distances discussed here, whereas the shorter one is considerably stronger. Further values come from the two structure types of pure *rare-earth triacetates*. In the structures of the Eu(OAc)$_3$-structure type the curve of the interatomic RE··· RE distances runs parallel with an offset of about −0.05 Å over the complete set of data [RE = Eu − Er], whereas the RE···RE distances in the Lu(OAc)$_3$-structure type [RE = Tm − Lu] are more than 1 Å longer.

d(RE···RE)$_{long}$ decreases with decreasing size of RE, too, up to minima in the range of RE = Sm, Eu, Gd. Thereafter, however, the values increase rapidly giving both curves the appearance of a sinusoidal function with a point of inflection around RE = Dy/Ho. For d(RE···RE)$_{long}$, the minimal and maximal values differ by 0.2557/0.2778 Å for Hal = Cl/Br. The complex behavior of this structural parameter is completely different from what one would expect from lanthanide contraction and is one of the strongest indicators to separate the whole dataset into two subsets for *e*RE and *l*RE as regression analyses work well only therein. Thus, values d(RE···RE)$_{long}$ can be described by use of a quadratic equation with high reliability [$R_{Cl/Br}$ = 0.9990/0.9987, concave] in the first subset, and [$R_{Cl/Br}$ = 0.9911/0.9989, concave] in the second subset. Looking into more detail, the decrease of d(RE···RE)$_{short}$ exhibits a similar, but very flat sigmoid curvature in the opposite direction to d(RE···RE)$_{long}$. Division of the corresponding data into two subsets results in somewhat better fits by quadratic equations ($R_{Cl/Br}$ = 0.9961/0.9989, concave, subset 1/$R_{Cl/Br}$ = 0.9950/9924, convex, subset 2) than the regression analysis over the complete set (see above).

The long RE···RE distances show in contrast to the short ones a significant impact from the size of the halide ion as they are shorter for Hal = Br for the larger RE atoms, whereas the situation inverts on the ascending branch of the curves with decreasing size of RE after a crossing point of both curves at RE = Dy.

The progress of the angles between the RE atoms exhibits a behavior inverse to the behavior of the long RE···RE distances: first, they increase with decreasing size of RE up to maxima around RE = Sm, Eu, Gd, then the values decrease rapidly up to Lu giving the complete curve a sinusoidal appearance with a point of inflection around RE = Ho. As before, the progress of this parameter can be explained quite well by splitting the whole dataset into two different subsets. Regarding the two subsets, the values in the *e*RE subset differ by 1.01°/1.27° and those in the *l*RE subset by 5.37°/5.67°. Within the subsets, all curves can be fit as usual with quadratic equations of quite good [$R_{Cl/Br}$ = 0.9684/0.9731, *e*RE subset, concave] to very good [RCl/Br = 0.9971/0.9950, *l*RE subset, convex] reliability factors.

3.3. RE Coordination

Further information on the interaction of lanthanide contraction, halide size, and atom arrangement comes from the coordination sphere around the RE atoms. This coordination sphere only consists of oxygen atoms, delivered from three water molecules and two acetate anions. The corresponding RE-O distances are summarized in Table 3 and visualized as a function of increasing atomic number *Z* of RE in Figure 7.

RE-O distances for a given RE element cover ranges of 0.316/0.329 Å for RE = $Ce_{Cl/Br}$, and 1.018/1.050 Å for RE = $Lu_{Cl/Br}$. Although most of the different RE-O distances decrease with increasing *Z* of RE, i.e., the shortest one [RE-O(11)], by 0.229 Å for both halides, the longest ones, [RE-O(11)^1], first decrease, too, up to minima at RE = Eu before they increase again giving the curves a similar sigmoid shape as observed for d(RE···RE)$_{long}$ (see above). From Ce to Lu these bonds become longer by 0.473 Å for Hal = Cl and 0.492 Å for Hal = Br. As a result, the coordination number of RE decreases from CN9 for Ce to CN8 for Lu accompanied by a change of the coordination polyhedra from distorted, monocapped square antiprismatic for Ce to distorted, bicapped trigonal prismatic for Lu (Figure 8). In this context, it seems advised to speak of two different structure types, represented by the

atom arrangement of these two RE elements. Both structure types are correlated to each other in the way that the structural parameters of the Ce-structure type change in direction.

Table 3. RE-O distances [Å] with standard deviations in parentheses of the $RE(OAc)_2Hal{\cdot}3H_2O$ compounds with Hal = Cl, Br.

RE	Ce	Pr	Nd	Pm	Sm	Eu	Gd	Tb	Dy	Ho	Er	Tm	Yb	Lu
Hal = Cl														
RE(1)-O(11)	2.422(2)	2.404(1)	2.390(1)		2.351(1)	2.341(1)	2.325(1)	2.294(1)	2.274(1)	2.252(1)	2.232(2)	2.218(1)	2.201(2)	2.193(1)
RE(1)-O(21)	2.440(2)	2.422(1)	2.406(1)		2.373(1)	2.362(1)	2.346(1)	2.323(1)	2.312(1)	2.295(1)	2.280(2)	2.265(1)	2.246(2)	2.239(1)
RE(1)-O(2W)	2.486(2)	2.468(1)	2.452(1)		2.421(1)	2.407(1)	2.393(1)	2.403(1)	2.361(2)	2.345(1)	2.331(2)	2.320(1)	2.312(2)	2.302(2)
RE(1)-O(3W)	2.499(2)	2.482(1)	2.467(1)		2.438(1)	2.427(1)	2.418(1)	2.403(1)	2.392(1)	2.381(1)	2.372(2)	2.360(1)	2.347(2)	2.346(2)
RE(1)-O(1W)	2.524(2)	2.506(1)	2.487(1)		2.457(1)	2.444(1)	2.425(1)	2.404(1)	2.388(1)	2.367(1)	2.346(2)	2.339(1)	2.320(2)	2.309(2)
RE(1)-O(12) [1]	2.536(2)	2.516(1)	2.498(1)		2.462(1)	2.450(1)	2.436(1)	2.413(1)	2.396(2)	2.378(1)	2.362(2)	2.346(1)	2.334(2)	2.327(2)
RE(1)-O(22) [2]	2.548(2)	2.529(1)	2.510(1)		2.475(1)	2.462(1)	2.449(1)	2.428(1)	2.416(1)	2.400(1)	2.386(2)	2.373(1)	2.359(2)	2.358(2)
RE(1)-O(21) [2]	2.665(2)	2.648(1)	2.633(1)		2.620(1)	2.613(1)	2.607(1)	2.612(1)	2.604(1)	2.596(1)	2.588(2)	2.592(1)	2.601(2)	2.585(2)
RE(1)-O(11) [1]	2.738(2)	2.725(1)	2.706(1)		2.723(1)	2.728(1)	2.740(1)	2.820(1)	2.905(2)	2.991(1)	3.083(2)	3.128(2)	3.178(2)	3.211(2)
Hal = Br														
RE(1)-O(11)	2.417(1)	2.401(1)	2.388(1)		2.349(2)	2.338(1)	2.324(2)	2.294(2)	2.269(1)	2.248(2)	2.229(1)	2.216(2)	2.201(2)	2.188(2)
RE(1)-O(21)	2.431(1)	2.416(1)	2.403(1)		2.370(2)	2.356(1)	2.343(2)	2.322(1)	2.307(1)	2.294(2)	2.280(1)	2.266(1)	2.251(1)	2.238(2)
RE(1)-O(2W)	2.489(1)	2.471(1)	2.457(1)		2.425(2)	2.409(2)	2.398(2)	2.381(2)	2.365(1)	2.346(2)	2.338(1)	2.325(2)	2.316(2)	2.305(2)
RE(1)-O(3W)	2.490(2)	2.476(1)	2.461(1)		2.431(2)	2.420(2)	2.412(2)	2.398(2)	2.386(2)	2.366(2)	2.347(2)	2.353(2)	2.344(2)	2.338(2)
RE(1)-O(1W)	2.526(1)	2.504(1)	2.490(1)		2.459(2)	2.442(2)	2.426(2)	2.405(2)	2.389(1)	2.373(2)	2.360(2)	2.336(2)	2.322(2)	2.306(2)
RE(1)-O(12) [1]	2.536(1)	2.516(2)	2.499(1)		2.466(2)	2.450(2)	2.439(2)	2.417(2)	2.395(2)	2.376(2)	2.365(2)	2.342(2)	2.333(3)	2.323(2)
RE(1)-O(22) [2]	2.539(1)	2.527(1)	2.504(1)		2.471(2)	2.459(2)	2.447(2)	2.429(2)	2.412(2)	2.395(2)	2.382(1)	2.368(2)	2.358(2)	2.350(2)
RE(1)-O(21) [2]	2.666(1)	2.652(1)	2.632(1)		2.623(2)	2.615(1)	2.608(2)	2.612(2)	2.603(1)	2.591(2)	2.582(1)	2.587(2)	2.594(2)	2.577(2)
RE(1)-O(11) [1]	2.746(1)	2.730(1)	2.711(1)		2.722(2)	2.720(2)	2.733(2)	2.808(2)	2.917(2)	3.026(2)	3.129(2)	3.165(2)	3.213(2)	3.238(2)

Symmetry transformations used to generate equivalent atoms: (1) −x, −y + 1, −z + 1; (2) −x + 1, −y + 1, −z + 1.

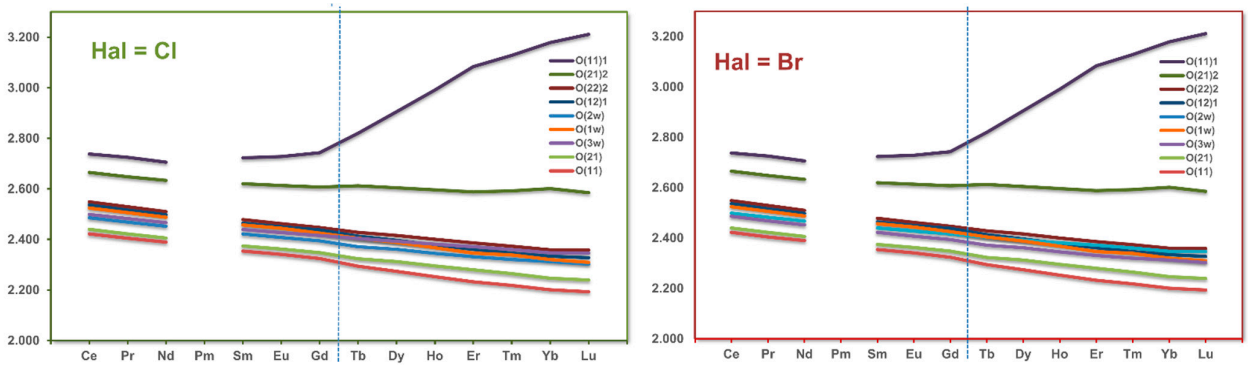

Figure 7. Overview on the evolution of the RE-O distances [Å] in $RE(OAc)_2Cl{\cdot}3H_2O$ with RE = Ce-(Pm)-Lu and Hal = Cl, Br; Symmetry transformations used to generate equivalent atoms: (1) −x, −y + 1, −z + 1; (2) −x + 1, −y + 1, −z + 1; for reasons of clarity all curves are drawn over the complete datasets without interruption at the borderline (blue) between of early and late RE elements.

Again, quadratic regression analyses work quite well when splitting the dataset and fitting the data of both subsets separately. Parameters of the resulting equations and reliability factors R are given in Figure S10 for d(RE···OAc) and in Figure S11 for $d(RE{\cdots}H_2O)$.

Besides this general trend, the data provide an interesting feature highlighting the transition between both coordination polyhedra at the common border of both subsets. To recognize this feature, the evolution of the RE-O distances with decreasing size of RE has to be analyzed in more detail looking separately at the RE-H_2O distances (Figure 9).

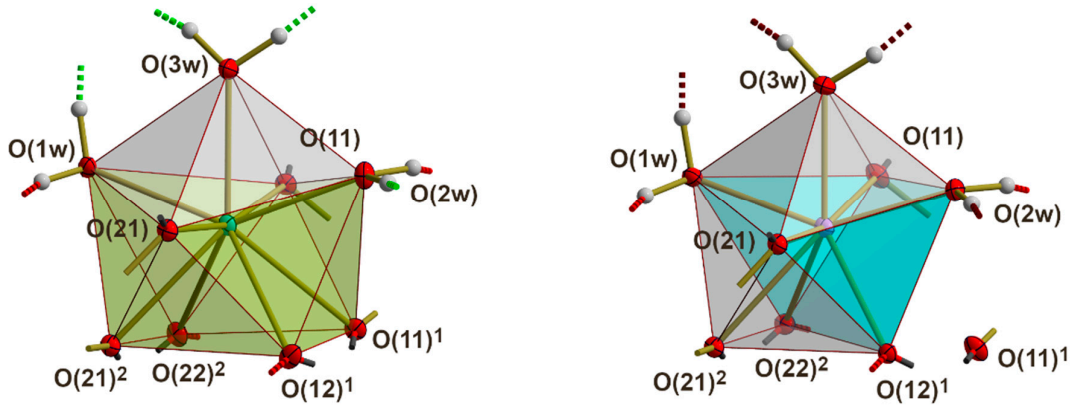

Figure 8. Distorted monocapped square-antiprismatic, ninefold coordination of RE = Ce_{Cl} (**left**) and distorted bicapped trigonal prismatic, eightfold coordination of RE = Lu_{Br} (**right**); color codes: caps = grey, square antiprism = green, trigonal prism = blue; hydrogen bonds are indicated by short dashed sticks with color codes: -OH···O = red, -OH···Cl = green, -OH···Br = brown; symmetry codes used to generate equivalent atoms: (^{1}) −x, −y + 1, −z + 1; (^{2}) −x + 1, −y + 1, −z + 1.

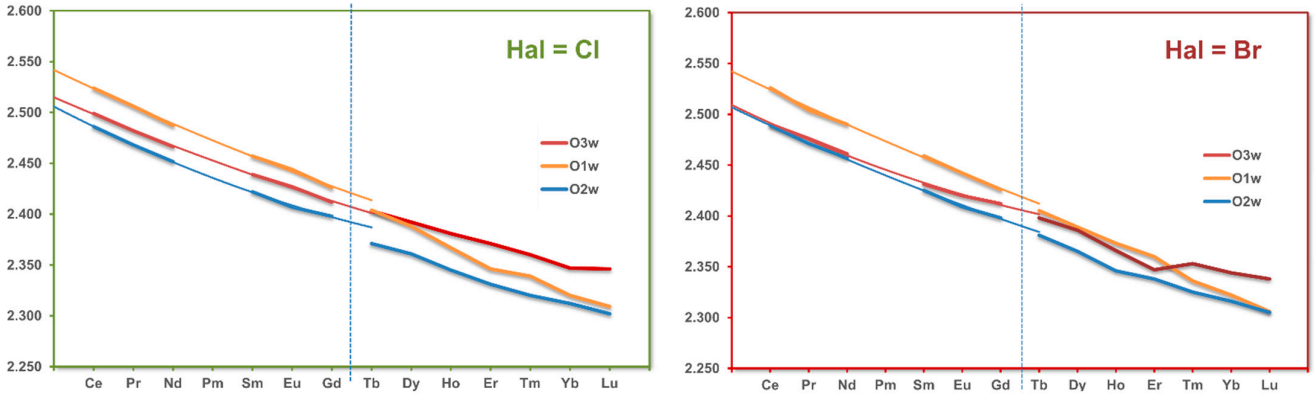

Figure 9. Overview of the evolution of the RE-H_2O distances [Å] in $RE(OAc)_2Hal{\cdot}3H_2O$ compounds with Hal = Cl (**left**) and Hal = Br (**right**); the connecting line between both subsets has been omitted as have been added the lines of regression analysis in case of the early RE elements in order to show the jumps of the properties.

In both polyhedra, the three water molecules act as monodentate ligands. Therefore, one might expect that the corresponding bond lengths decrease continuously and uniformly from Ce to Lu, in accordance with lanthanide contraction and with the observation in several other classes of isostructural compounds such as the *nonahydrate triflates* and *ethylsulfates* mentioned above. In the present case, however, two significant alterations can be deduced from Figure 9: (*i*) there is a significant jump in the bond lengths between the first (*e*RE, Ce-structure) and second subset (*l*RE, Lu-structure type), and (*ii*) the RE···H_2O_1 bond becomes much stronger/shorter with increasing *Z* than the two other RE···H_2O bonds in the *l*RE-subset. At the right end (RE = Lu) of the RE elements this bond is as strong/short as the RE···H_2O_2 bond.

This behavior corresponds very well with the fact that the oxygen atom of H_2O_1 occupies a position in the coordination sphere of RE just opposite to $O(11)^1$ of OAc_1. In the way this oxygen moves out of the RE coordination sphere (with decreasing size of RE) the stronger becomes the RE···H_2O_1 bond.

3.4. Coordination Modes of the Acetate Ligands

Both acetate groups act as bidentate, bridging ligands independently from whether the coordination number is 8 or 9. Differences in coordination numbers result from the fact that one acetate group (OAc_2) acts as a chelating ligand over the complete series of RE

elements, in contrast to the other one (OAc_1), which loses this chelating function with decreasing size of RE (Figure 10a).

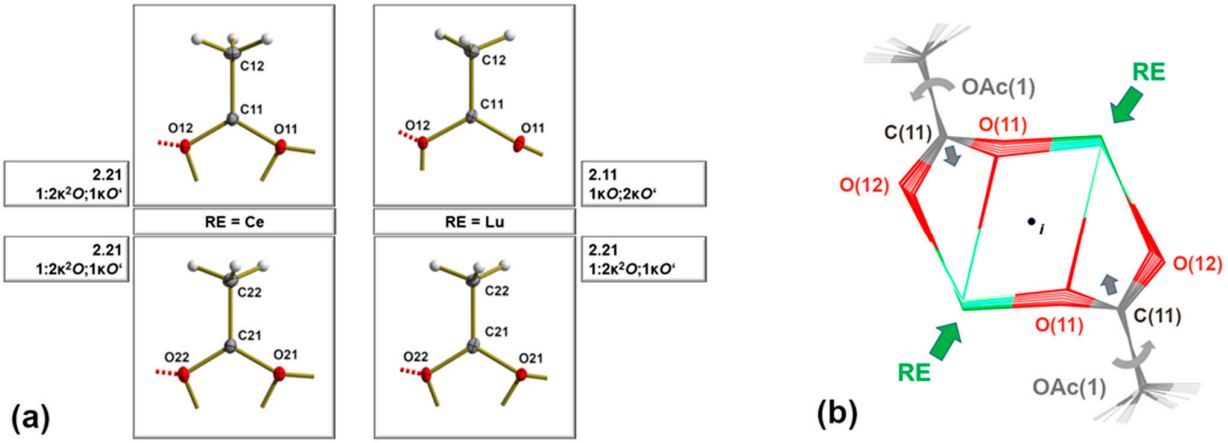

Figure 10. (**a**) Ball-and-stick model of the two extreme acetate coordination in the series of $RE(OAc)_2Hal{\cdot}3H_2O$ compounds (Hal = Cl, RE = Ce (left of a), RE = Lu (right of a); bonds from oxygen to the two RE atoms are indicated by shortened sticks, hydrogen bonds by short, dashed sticks in red. (**b**) Schematic stick model showing the motion of OAc_1 in the metal-oxygen plane with respect to the common inversion center.

Besides the above-mentioned global view on the RE-OAc bond lengths, a detailed inspection of bond lengths and angles within the acetate groups will give a deeper insight into the structural evolution within both structure types as a consequence of lanthanide contraction. In the following, we will use the Harris symbol as described by Coxall et al. [20] for the different acetate coordination modes to distinguish the two different crystallographic acetate ligands shown in Figure 10a. The first one (atoms labeled 1n) exhibits a bridging 2.11 ($1\kappa O; 2\kappa O'$) coordination mode. In addition, these acetate ligands act as hydrogen acceptors in hydrogen bonds.

Bond lengths and angles within the acetate groups are listed in Table S4. C-C bonds only slightly vary in the range of the standard deviations. For OAc_2 they are in general a little bit shorter [$\bar{d}$(C(21)-C(22)$_{Cl/Br}$ = 1.490(4)/1.492(2) Å] than for OAc_1 [$\bar{d}$(C(11)-C(12)$_{Cl/Br}$ = 1.494(3)/1.496(3) Å].

In OAc_2 the two different C-O bonds differ on average by 0.020/0.022 Å [Cl/Br] with the longer/weaker [$\bar{d}_{Cl/Br}$O(21)-C(21) = 1.279(2)/1.279(2) Å] bonds to O(21) and the shorter/stronger [$\bar{d}_{Cl/Br}$O(22)-C(21) = 1.259(3)/1.257(2) Å] one to O(22), both less affected from the size of the RE^{3+} ion are negligible as the standard deviations show (Figure S11). Bond angles in these acetate groups (Figure S12) are unaffected by lanthanide contraction only in the case of the O(22)-C(21)-C(22) bond angles, the angles opposite to the bridging RE atoms [$\bar{d}_{Cl/Br}$(∠O(21)-C(21) = 121.2(2)°/120.0(3)°]. On the other hand, bond angles between both oxygen atoms decrease by 1.5°/0.6° from $Ce_{Cl/Br}$ [119.0(2)°/119.3(2)°] to $Lu_{Cl/Br}$ [117.5(2)°/118.2(3)°] and increase the bond angles O(21)-C(21)-C(22) by 1.4°/0.5° from $Ce_{Cl/Br}$ [119.7(2)°/120.1(2)°] to $Lu_{Cl/Br}$ [121.1(3)°/120.6(3)°] in this acetate ligand.

In Oac_1, the O-C bonds are strongly correlated with the coordination behavior of the acetate groups. Thus, the bonds between O(12) and C(11) increase in length with the increasing length of the chelate bond. The slight increase finds expression when calculating the standard deviations of the mean values [$\bar{d}_{Cl/Br}$(O12)-C(11) = 1.261(3)/1.261(5) Å]. In contrast, bonds between O(22) and C(11) become shorter/stronger [d_{Cl}(O12-C11)$_{Ce\text{-}Lu}$ = 1.273(3) − 1.257(2) Å/d_{Br}(O12-C11)$_{Ce\text{-}Lu}$ = 1.273(3) − 1.2534) Å,] with decreasing size of RE^{3+} featuring a sigmoid curve inverse to the sigmoid curve of the corresponding RE-O(11)[1] bonds of Figure 7. From RE = Ho up to RE = Lu, this bond is stronger than the second C-O bond as a result of the loss of the chelate function. In Oac_1, the bond angles (Figure S12) increase between the oxygen atoms [$\angle_{Cl/Br}$(O11-C11-O12)] by 1.9°/2.4° from

$Ce_{Cl/Br}$ [119.5(2)°/119.3(2)°] to $Lu_{Cl/Br}$ [121.4(2)°/121.7(3)°] also as a result of the loss of the chelate function. To the same extent [1.9°/2.2°] as the bond angles O(12)-C(11)-C(12), the bond angles opposite to the O-RE bridges decrease. Only the bond angles between O(22) and C(22) remain almost constant [$_{Cl/Br}$(O12-C11-C12) = 120.6(2)°/120.6(2)°] over the complete series of RE elements.

Weakening and loss of the chelating function is accompanied by a movement of the acetate group OAc_1 as a whole as visualized in Figure 10b. With decreasing size of the RE atom the acetate groups perform a rotation in the plane of the metal and oxygen atoms so that the RE-O(11)[1] bonds lose their chelate function. This rotation is accompanied by a movement of the methyl group in the direction of the central part of the coordination polymer. In some cases (see above: Single crystals X-ray structure determination), this movement opens additional space for a second orientation of this methyl group.

A significant influence of the halide ions and their sizes on the structure parameters of the acetate ligand is not recognizable. Changes of bond angles in the two different acetate groups of $RE(OAc)_2Cl{\cdot}3H_2O$ as a function of *Z* of RE are visualized in Figure 11.

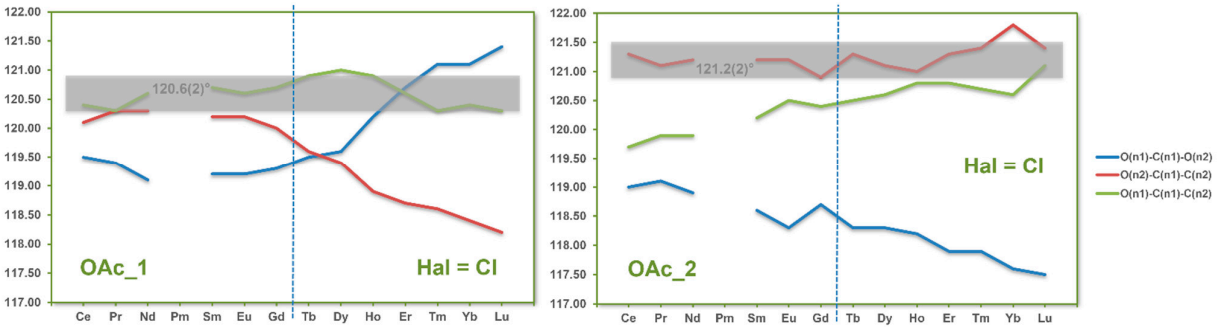

Figure 11. Changes of bond angles [°] in the two different acetate groups of $RE(OAc)_2Cl{\cdot}3H_2O$ as a function of decreasing size of RE; mean values are indicated by broad, the standard deviations simulating bars (grey).

3.5. Hydrogen Bonds

In addition to coordinative RE-O and electrostatic anion-cation interactions, there exist hydrogen bonds between the water molecules and halide ions. Some specific data characterizing these hydrogen bonds are summarized in Table S4.

-OH···O hydrogen bonds are restricted to water molecules between neighboring RE-atoms alongside the surface of the coordination polymer (Figure 3). Accordingly, they are responsible—besides the μ_2-acetate groups—for the constitution of the coordination polymer but also depend on lanthanide contraction and the alignment of the RE atoms. With $\overline{d}$(O···O)$_{Cl/Br}$ = 2.707(3)/2.708(4) Å the hydrogen bonds [O(1w)···O(12)[4]] alongside the short RE···RE distances are relatively strong and almost independent from lanthanide contraction and size of the halide ion (Figure S12). Moreover, these hydrogen bonds are of similar strength in both subsets.

By way of contrast, the O···O distances alongside the long RE···RE distances [O(2w)···O(22)[5]] depend on the size of the halide ion [Br < Cl] (Figure 12).

In addition, they are longer than the former one [especially for Hal = Cl and RE = Ce, Δ(O···O)$_{long\text{-}short}$ = 15 pm], and decrease in length/becomes stronger in the case of the early RE elements [Δ(O···O)$_{Cl/Br}$ = 15/10 pm] as the distances between the metal atoms increase (Figure 6). In the case of the late RE elements most of these hydrogen bonds, Hal = Cl as well as Hal = Br, are stronger than the previous one in the same subset whereas their variations follow similar trends. In the first subset, the regression analyses of these O···O distances show less accuracies [R = 0.9611–0.9958], for the late RE elements the corresponding values spread around a mean value of 2.698(3)/2.705.4(4) Å for Hal = Cl/Br.

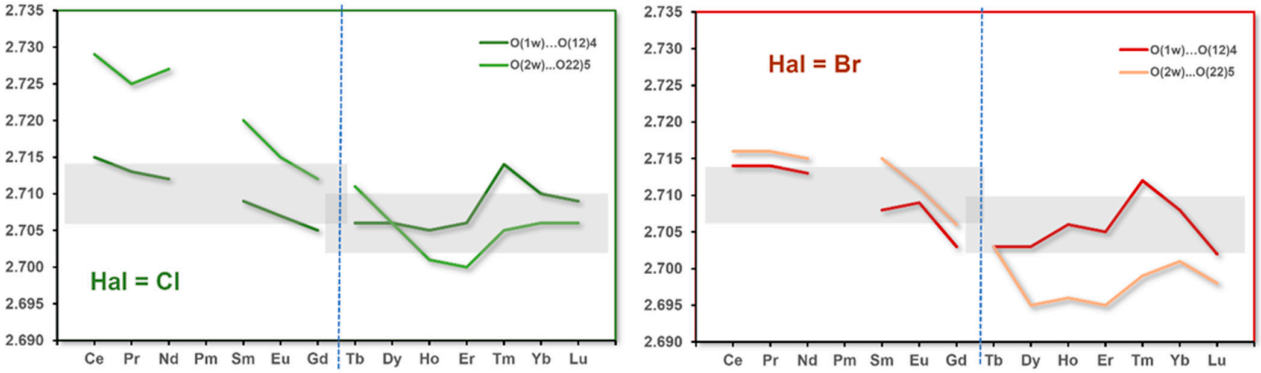

Figure 12. Progress of the interatomic d(O···O) distances [Å] in the hydrogen bonds between the water molecules; mean values are indicated by broad, the standard deviations simulating bars (grey); symmetry transformations used to generate equivalent atoms: (4) x + 1, yes, z; (5) x − 1, y, z.

Additional hydrogen bonds exist between the water molecules of the coordination polymer and the laterally located halide ions. Changes of O···Hal distances of these hydrogen bonds are depicted in Figure 13 as a function of Z.

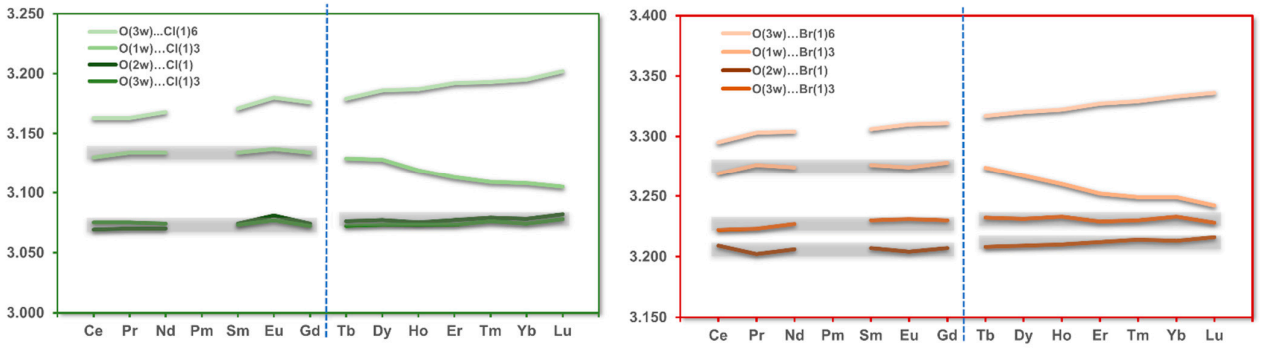

Figure 13. Progress of interatomic O···Hal [Å] distances in the hydrogen bonds between the water molecules and halide anions (Hal = Cl left, Hal = Br, right) as a function of Z; mean values are indicated by broad, the standard deviations simulating bars (grey); symmetry transformations used to generate equivalent atoms: (3) x, y − 1, z; (6) −x + 1/2, y − 1/2, −z + 3/2.

In the subset of *e*RE, the O···Hal distances only slightly increase with *Z*. With the exception of the longest/weakest hydrogen bond [O3w···Hal^{6} = 3.170(7)/3.305(6) Å], variations in bond lengths are small, which is why it seems justified to describe these hydrogen bonds by use of mean values [$\overline{d}$(O3w···Cl^{3}/Br^{3}) = 3.073(4), 3.074(2) Å, $\overline{d}$(O2w···Cl/Br) = 3.134(2)/3.206(2) Å, and $\overline{d}$(O1w···Cl^{3}/Br^{3}) = 3.274(4), 2.275(3) Å]. With respect to the halide ion, the differences between the two strongest hydrogen bonds are only marginal [0.001 Å] for Hal = Cl, but significant [0.021 Å] for Hal = Br.

Some other trends are observed in the case of the O···Hal distances in the subset of *l*RE. Although the two strongest/shortest hydrogen bonds slightly increase [0.006,0.006/0.008, 0.004 Å, Hal = Cl/Br] with decreasing size of the RE^{3+} ion, the weakest/longest one increases significantly [0.023/0.019 Å]. A completely different behavior is found in the case of the second weakest hydrogen bonds as their values decrease markedly, more expressed for Hal = Br [0.046 Å] than for Hal = Cl [0.024 Å]. All changes described result from lanthanide contraction, and its influence on the RE alignment and coordination including the positions of the water molecules that directly influence the stacking of the coordination polymers within the ab-plane and in the c-direction as the discussion on the variation of the lattice parameters with decreasing size of RE documented (see above).

3.6. Packing

In summary, the one-dimensional coordination polymers constitute linear rods with an elliptical cross-section, constricted in the middle to some extent (Figure 14). Its surfaces consist alternately of apolar methyl groups and polar water molecules. The latter are involved in -OH O hydrogen bonds alongside the rods or hydrogen bonds to the halide ions.

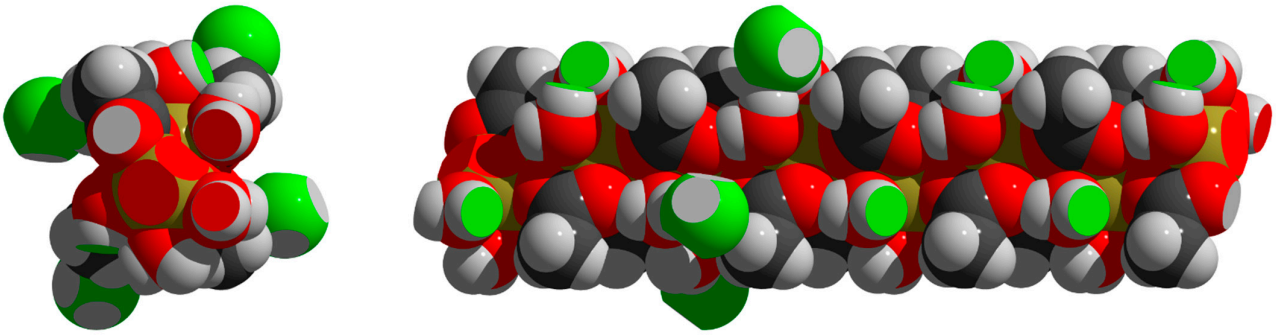

Figure 14. Space-filling model showing a detail (cross-section, looking down the a-axis **left**, side view **right**) of the one-dimensional coordination polymer in the crystal structures of $RE(OAc)_2Hal{\cdot}3H_2O$ compounds (here: RE = Ce, Hal = Cl); color code: oxygen = red, carbon = black, hydrogen = white, cerium = brassy; r_{vdW}: O = 1.52, C = 1.65, H = 1.2, Ce = 2.2, Cl = 1.75 Å; interactions with additional atoms are visualized by cutting off the overlapping cap and coloring the interface using the color of the auxiliary atom.

The interaction of these rods (Figure 15) via the hydrogen bonds with the halide ions results in their sheet-like arrangement within the ab-plane and the stacking of these sheets in the direction of the c-axis with the monoclinic angle ß.

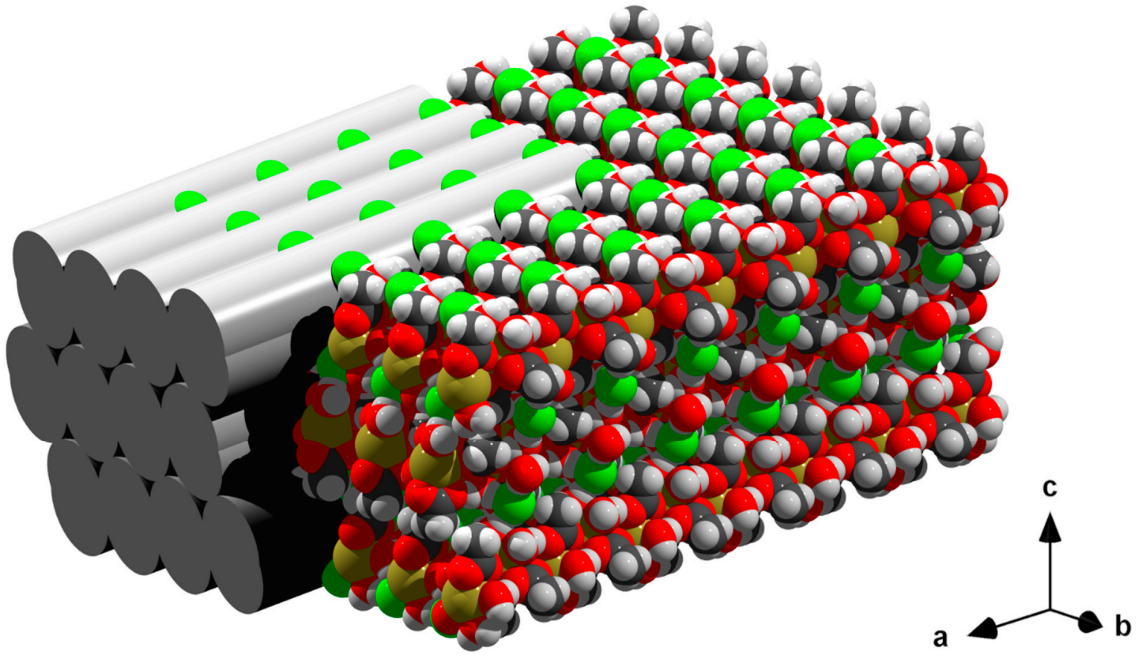

Figure 15. Space-filling model showing a detail of the three-dimensional stacking of the one-dimensional coordination polymers (denoted as rods) in the crystal structures of $RE(OAc)_2Hal{\cdot}3H_2O$ compounds (here: RE = Ce, Hal = Cl); atom colors and sizes as in the previous figure.

4. Conclusions

Our SXRD data underline the important role of lanthanide contraction and size of the halide ion on the structural evolution in the series of isomorphous $RE(OAc)_2Hal{\cdot}3H_2O$

compounds and reveal the complex response of a given atom arrangement on these two variables.

Some parameters such as the unit cell volumes reflect the shrinkage of the rare-earth element throughout the complete series of compounds as confirmed by quadratic regression analyses whereas some others including lattice constants and most bond lengths and angles exhibit a more complex behavior often associated with sigmoid curves. These findings are best described by separating the datasets into two subsets, one with the data of the early RE elements and one with the data for the late RE elements. As a result, most of the data in the individual datasets can be simulated with high reliability using quadratic regression analyses often with different curvatures (concave/convex) in the two datasets. Both subsets are represented by different structure types, the Ce-structure type in case of the early RE elements and the Lu-structure type in case of the late ones, both with structure parameters that converge towards each other with decreasing/increasing RE^{3+} radius up to the borderline between both groups of elements giving rise to a continuous transition from CN9, distorted monocapped square antiprismatic for the Ce-structure type to CN8, distorted bicapped trigonal prismatic for the Lu-structure type. These and many other structural changes are facilitated by the flexibility of the RE alignment within the non-linear, one-dimensional coordination polymer to adjust both the lanthanide contraction and the spatial requirements of the hydrogen bonds to the halide ions. Moreover, our data show that the reduction of the coordination number as a consequence of lanthanide contraction is accompanied by the loss of the chelate function of one of the two acetate groups with a strong influence on its internal structure parameters and on the free rotation of its methyl group.

Supplementary Materials: The following supporting information can be downloaded at: https://www.mdpi.com/article/10.3390/cryst13071043/s1, Table S1: RE_{atom} and RE^{3+} ionic radii; Figure S1: MIR spectrum of $Tb(OAc)_2Br{\cdot}3H_2O$; Figure S2: Raman spectrum of $Tb(OAc)_2Br{\cdot}3H_2O$, Figure S3: Unit cell volume and linear fit, Figure S4: $\Delta V(\text{linear}) = V_{obs} - V_{calc}$, Figure S5: $\Delta V(\text{quadratic}) = V_{obs} - V_{calc,}$, Figure S6: c-axis, Figure S7: b-axis, Figure S8: angle ß, Table S2: Structural data of RE···RE interaction, Figure S9: d(RE···RE) with additional data, Figure S10: RE-OAc bond lengths, Figure S11: RE-H_2O bond lengths and quadratic regression analyses, Table S3: Bond lengths and angles within acetate groups, Figure S12: OAc bond lengths, Figure S13: OAc bond angles, Table S4: data of hydrogen bonds.

Author Contributions: Conceptualization, M.H. (Markus Haase), and H.R.; resources, M.B. (Hal = Cl) and M.H. (Maik Horstmann) (Hal = Br); original draft preparation, H.R.; visualization, H.R.; funding acquisition, M.H. All authors have read and agreed to the published version of the manuscript.

Funding: This research was funded by the Deutsche Forschungsgemeinschaft, HA 1649/7-1.

Institutional Review Board Statement: Not applicable.

Informed Consent Statement: Not applicable.

Data Availability Statement: Data is contained within the article or Supplementary Materials.

Acknowledgments: We thank the Deutsche Forschungsgemeinschaft and the Government of Lower-Saxony for funding the diffractometer and acknowledge support by Deutsche Forschungsgemeinschaft (DFG).

Conflicts of Interest: The authors declare no conflict of interest.

References

1. Holleman/Wiberg-Anorganische Chemie. *Nebengruppenelemente, Lanthanoide, Actinoide, Transactinoide-Table V*, 103rd ed.; Wiberg, N., Ed.; Walter de Gruyter: Berlin, Germany; Boston, MA, USA, 2016; Volume 2.
2. Shannon, R.D. Revised Effective Ionic Radii and Systematic Studies of Interatomie Distances in Halides and Chalcogenides. *Acta Cryst.* **1976**, *A32*, 751–767. [CrossRef]
3. Gerkin, R.E.; Reppart, W.J. The structures of the lanthanide ethyl sulfate enneahydrates, $M(C_2H_5SO_4)_3.9H_2O$ [*M* = La -Lu (except Pm), at 171 K. *Acta Cryst.* **1984**, *C40*, 781–786. [CrossRef]

4. Chatterjee, A.; Maslen, E.N.; Watson, K.J. The Effect of Lanthanoid Contraction on the Nonaaqualanthanoid(III) Tris(trifluoromeths anesulfonates). *Acta Cryst.* **1988**, *B44*, 381–386. [CrossRef]
5. Junk, P.C.; Kepert, C.J.; Wei-Min, L.; Skelton, B.W.; White, A.H. Structural Systematics of Rare Earth Complexes. X. ('Maximally') Hydrated Rare Earth Acetates. *Austr. J. Chem.* **1999**, *52*, 437–457. [CrossRef]
6. Arias, J.L.; Cabrera, A.; Sharma, P.; Rosas, N.; Garcia, J.L.; Hernandez, S. Catalytic auto-condensation of 2,4-pentanedione promoted by Sm(III) acetylacetonate: The X-ray strcutre of a novel complex $[Sm(CH_3COO)_3(H_2O)_2](H_2O)_2$. *Inorg. Chim. Acta* **2000**, *310*, 261–264. [CrossRef]
7. Yu, Q.; Zhou, X.; Liu, M.; Chen, J.; Zhou, Z.; Yin, X.; Cai, Y. Syntheses, characterization, and luminescence of two lanthanide complexes $[Ln_2(acetate)_6(H_2O)_4]\cdot 4H_2O$ (Ln = Tb(1), Sm(2)). *J. Rare Earth* **2008**, *26*, 178–184. [CrossRef]
8. Lossin, A.; Meyer, G. Wasserfreie Selten-Erd-Acetate, $M(CH_3COO)_3$ (M = Sm-Lu, Y) mit Kettenstruktur. Kristallstrukturen von $Lu(CH_3COO)_3$ und $Ho(CH_3COO)_3$. *Z. Anorg. Allg. Chem.* **1993**, *619*, 1609–1615. [CrossRef]
9. Lossin, A.; Meyer, G. Dimers and chains in lanthanide acetate-chloride hydrates $[M(CH_3COO)_2(H_2O)_3]Cl$ (M = Ce-Lu, Y) and $[M(CH_3COO)(H_2O)_6]Cl_2\ H_2O$ (M = La-Sm): A survey of their synthesis, crystal chemistry and thermal decomposition. *J. Less Common Met.* **1991**, *175*, 301–308. [CrossRef]
10. Schleid, T.; Meyer, G. Synthese und Kristallstruktur von Europium(III)-diacetatotriaquo-chlorid, $[Eu(CH_3COO)_2(H_2O)_3]Cl$. *Z. Naturforsch.* **1989**, *44b*, 1007–1010. [CrossRef]
11. Cesur, N.; Pantenburg, I.; Meyer, G. Crystal structure of *catena*-[triaqua-bis(acetato-*O,O'*)gadolinium(III)]chloride, $[Gd(CH_3COO)_2(H_2O)_3Cl$. *Z. Kristallogr. New Cryst. Struct.* **2005**, *220*, 631–632. [CrossRef]
12. Chen, W.-T.; Luo, Z.-G.; Yao, Z.-L. Synthesis, crystal structure and fluorescense of an unusual terbium carboxylate. *Acta Chim. Slov.* **2012**, *59*, 949–953. [PubMed]
13. Haase, M.; Rissiek, P.; Gather-Steckhan, M.; Henkel, F.; Reuter, H. Structural Evolution in the $RE(OAc)_3\cdot 2AcOH$ Structure Type. A Non-Linear, One-Dimensional Coordination Polymer with Unequal Interatomic Rare Earth Distances. *Crystals* **2021**, *11*, 768. [CrossRef]
14. Sheldrick, G.M. A short history of SHELX. *Acta Cryst.* **2015**, *C71*, 3–8. [CrossRef]
15. Spek, A.L. checkCIF validation ALERTS: What they mean and how to respond. *Acta Cryst.* **2020**, *E76*, 1–11. [CrossRef] [PubMed]
16. Brandenburg, K. *Diamond-Crystal and Molecular Visualization*; Crystal Impact: Bonn, Germany, 2006.
17. Macrae, C.F.; Bruno, I.J.; Chisholm, J.A.; Edgington, P.R.; McCabe, P.; Pidcock, E.; Rodriquez-Monge, L.; Taylor, R.; van de Streek, J.; Wood, P.A. Mercury CSD 2.0-new features for the visualization and investigation of crystal structures. *Appl. Crystallogr.* **2008**, *41*, 466–470. [CrossRef]
18. *POV-Ray: The Persistence of Vision Retracer*; Pty. Ltd.: Victoria, Australia, 2004.
19. Jordan, R.B. Lanthanide Contraction: What is Normal? *Inorg. Chem.* **2023**, *62*, 3715–3721. [CrossRef] [PubMed]
20. Coxall, R.A.; Harris, S.G.; Hernderson, D.K.; Parsons, S.; Takser, P.A.; Winpenny, E.P. Inter-ligand reactions: In situ formation of new polydentate ligands. *J. Chem. Soc. Dalton Trans.* **2000**, 2349–2356. [CrossRef]